Heterogeneous Catalysis

DOI: 10.1002/anie.200903918

Water-Gas Shift Reaction on a Highly Active Inverse CeO_x/Cu(111) Catalyst: Unique Role of Ceria Nanoparticles**

José A. Rodriguez, Jesús Graciani, Jaime Evans, Joon B. Park, Fan Yang, Dario Stacchiola, Sanjaya D. Senanayake, Shuguo Ma, Manuel Pérez, Ping Liu, Javier Fdez. Sanz, and Jan Hrbek*

The water-gas shift (WGS, $CO + H_2O \rightarrow CO_2 + H_2$) is an important reaction frequently used in the chemical industry for the production of clean H_2.[1] Oxide-supported copper catalysts show significant water-gas shift activity but their performance is not fully understood and is highly dependent on the synthesis conditions or the nature of the oxide support.[1–4] Either metallic Cu or Cu^+ cations have been proposed as active sites for the WGS.[1–8] In addition, the oxide support may not be a simple spectator and may play a direct role in the catalytic process.[1,4,9] Extended surfaces and nanoparticles of metallic copper are able to catalyze the WGS[3,5,6,10,11] and Cu(111) has become a benchmark surface for studying the WGS.[3,5,11–14] Specific rates, activation energies, and reaction orders are consistent with data reported for ZnO-supported Cu catalysts.[5,13] The rate-limiting step for the WGS on Cu(111) seems to be the dissociation of water,[11–13] and it is affected by the presence of surface modifiers such as S, O, or Cs.[13]

Herein, we investigate the WGS reaction on Cu(111) surfaces partially covered with ceria nanoparticles. Bulk ceria is a well known oxide support for WGS catalysts.[1,4,8,9] The CeO_x/Cu(111) system allows us to study in detail the role of the oxide in the catalytic process and, furthermore, catalysts with an inverse oxide/metal configuration have some advantages for practical applications.[15] Figure 1 shows images of scanning tunneling microscopy (STM) acquired after dosing Ce to Cu(111) at 650 K under an atmosphere of O_2 ($p \approx 5 \times 10^{-7}$ Torr). The reaction of O_2 with the Cu(111) substrate leads to formation of a layer of copper oxide which exhibits domains of different reconstructions of a Cu_2O(111) surface.[16] On top of the layer of copper oxide, there are two types of ceria features. These features were not seen in blank experiments for the adsorption of O_2 on Cu(111). In Figure 1, small islands of ceria (2–5 nm in size, CeO_x-I) appear on the terraces of the copper substrate, whereas large islands of ceria (30–50 nm in size, triangular shape, CeO_x-II) are embedded in the substrate step edges. Inside the large ceria islands, a moiré pattern can be seen with a separation of approximately 5 nm in between the depressions. The large ceria islands have a morphology different from that seen for the two most stable surfaces of bulk ceria: CeO_2(111) and CeO_2(110). An analysis of the structure of these islands reveals that they essentially have a height of 0.31 nm, which is consistent with a single layer of cerium sandwiched in between two layers of oxygen.[17] An O-Ce-O-Cu(interface) stacking is likely. The oxide nanoparticles in CeO_x/Cu(111) display a morphology quite different from that found before for the growth of ceria nanoparticles on a Au(111) substrate using the same deposition methodology.[17] In the CeO_x/Au(111) systems there were only large oxide islands at the step edges and these were exposing the (111) face of bulk ceria.[17] The interactions of

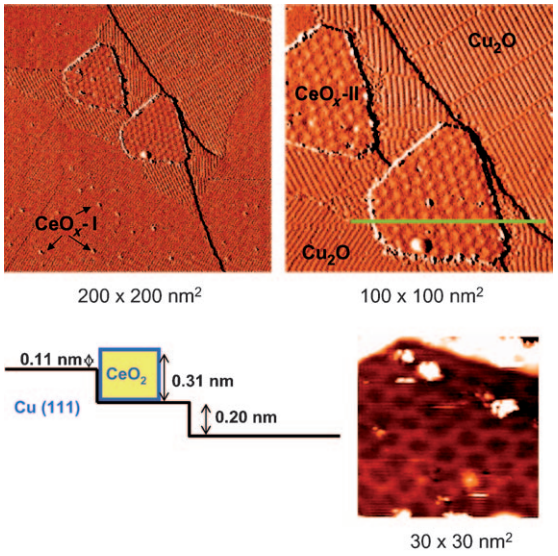

Figure 1. STM images recorded after dosing Ce to Cu(111) at 650 K under an atmosphere of O_2 ($p \approx 5 \times 10^{-7}$ Torr). The two differentiated images at the top were taken with $V_t = 3.1$ V and $I_t = 0.03$ nA. The height image at the bottom right, showing the inside of a ceria island, was taken at imaging conditions of 2.7 V, 0.05 nA. The scheme (bottom left) was composed using the line profile indicated by the green line shown near the middle of the top right image.

[*] Dr. J. A. Rodriguez, Dr. J. Graciani, Dr. J. B. Park, Dr. F. Yang, Dr. D. Stacchiola, Dr. S. D. Senanayake, Dr. S. Ma, Dr. P. Liu, Dr. J. Hrbek
Chemistry Department, Brookhaven National Laboratory
Upton, NY 11973 (USA)
Fax: (+1) 631-344-5815
E-mail: rodrigez@bnl.gov
Prof. J. Evans, Prof. M. Pérez
Facultad de Ciencias, Universidad Central de Venezuela
Caracas 1020A (Venezuela)
Prof. J. F. Sanz
Departamento de Química Física, Universidad de Sevilla
41012-Seville (Spain)

[**] The work performed at BNL was supported by the US Department of Energy, Office of Basic Energy Sciences, under contract DE-AC02-98CH10886. J.E. and M.P. are grateful to INTEVEP for partial support of the work carried out at the UCV. The work done at Seville was funded by MICINN, grant no MAT2008-04918 and the Barcelona Supercomputing Center—Centro Nacional de Supercomputación (Spain).

Supporting information for this article is available on the WWW under http://dx.doi.org/10.1002/anie.200903918.

the copper substrate with the ceria nanoparticles are much stronger allowing the existence of small oxide nanoparticles on terraces of the surface (CeO_x-I) and forcing a unique morphology on the large oxide particles (CeO_x-II).

Figure 2 displays typical Ce 3d X-ray photoelectron spectroscopy (XPS) and Cu L_3VV Auger spectra for a CeO_x/Cu(111) system in which 15–20% of the copper substrate was covered by ceria. For comparison, we also include the Ce 3d XPS spectra for nanoparticles of CeO_2 and Ce_2O_3 dispersed on a Au(111) substrate.[17,18] There are clear differences in the Ce 3d XPS line-shapes of the Ce^{3+} and Ce^{4+} oxidation states.[19] The as-prepared CeO_x/Cu(111) surface exhibits a Ce 3d XPS line shape where the features for Ce^{3+} dominate with some features for Ce^{4+} also present. Ce^{3+} sites are stable in unsupported ceria nanoparticles.[20] Density functional (DF) calculations for the deposition of a layer of CeO_2 on Cu(111), see below, point to a $Ce^{4+} \rightarrow Ce^{3+}$ reduction as a result of electronic interactions with the metal substrate.

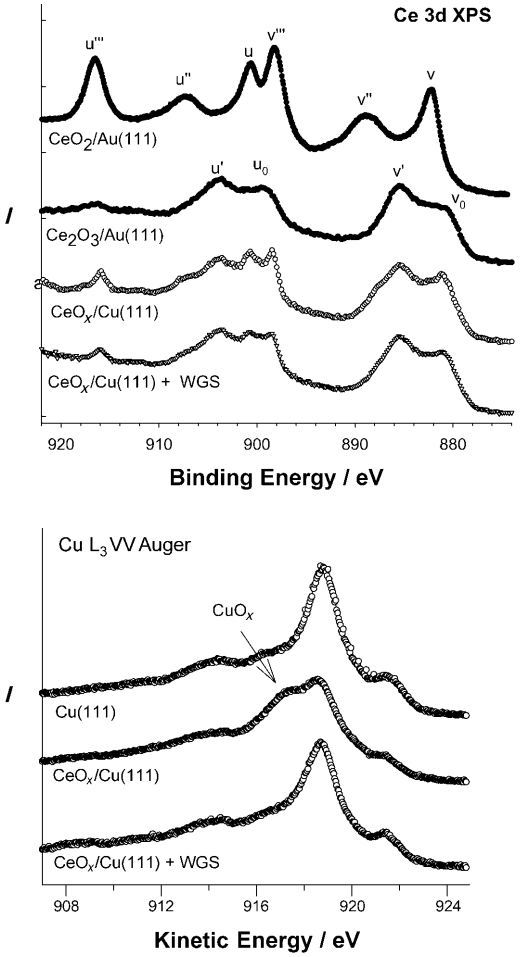

Figure 2. Top: Ce 3d XPS spectra acquired before and after exposing a CeO_x/Cu(111) surface to the reactants of the WGS (20 Torr of CO, 10 Torr of H_2O at 625 K for 5 min). The CeO_x/Cu(111) surface was prepared by dosing Ce to Cu(111) at 650 K under an atmosphere of O_2 ($p \approx 5 \times 10^{-7}$ Torr). The ceria covered 15–20% of the copper substrate. The Cs 3d XPS spectra for CeO_2/Au(111) and Ce_2O_3/Au(111) were taken from Ref. [18]. Bottom: Corresponding Cu L_3VV Auger spectra taken before and after exposing the CeO_x/Cu(111) surface to the reactants of the WGS.

Thus, the oxide nanoparticles in CeO_x/Cu(111) have a large concentration of Ce^{3+} sites, which makes them quite attractive for chemical and catalytic applications.[20]

The Cu L_3VV Auger spectra for the CeO_x/Cu(111) systems showed a line-shape (see bottom of Figure 2) that denoted the oxidation of the copper substrate.[21] The O_2 molecules present in the chamber environment during the deposition of Ce did oxidize the copper substrate, but we found that the layer of copper oxide formed could be reduced by reaction with CO at 550–650 K. After doing this, the recorded Cu L_3VV Auger spectra matched that of clean Cu(111) and in the Ce 3d XPS spectra there was a decrease in the amount of Ce^{4+} present. Figure 3 displays STM images for

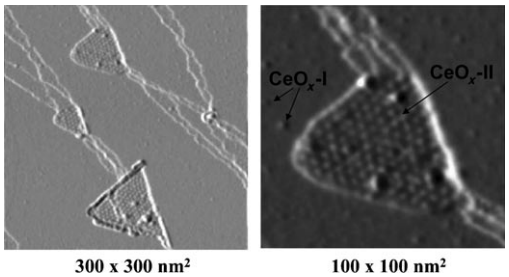

Figure 3. STM images taken after exposing a CeO_x/Cu(111) surface to 7.5×10^{-7} Torr of CO for 30 min at 650 K. STM parameters: $V_t = -1.2$ V, $I_t = 1$ nA. The two images were smoothed with a Gaussian filter.

a CeO_x/Cu(111) surface reduced in CO. The structural features characteristic of a layer of Cu_2O on Cu(111)[16] have disappeared. On the other hand, the small CeO_x-I and large CeO_x-II particles of ceria are still attached to the copper substrate.

Figure 4 shows the activities of Cu(111) and a CeO_x/Cu(111) system in which approximately 20% of the copper surface was covered by ceria. This was found to be the optimal ceria coverage for WGS activity. Copper surfaces with smaller or larger ceria coverages were less active. Furthermore, CeO_x/Cu(111) systems in which the copper substrate was totally covered by ceria displayed negligible WGS activity. The CeO_x nanoparticles supported on Cu(111) generated a catalyst that was 8-times (at 650 K) to 23-times (at 575 K) more active than the clean Cu(111) substrate. The data in Figure 4 were collected at temperatures of 575, 600, 625, and 650 K. Using the ln of the reaction rates, we constructed Arrhenius plots for CeO_x/Cu(111) and Cu(111). For comparison, we include results obtained under the same reaction conditions for Cu(100), and 0.5 ML of Cu deposited on CeO_2(111) and ZnO(000$\bar{1}$) surfaces.[22] The WGS on Cu(111) has an apparent activation energy of 0.78 eV, which is 0.1–0.2 eV larger than that found on Cu(100) and Cu(110).[3,5] In contrast, the apparent activation energy for the WGS on CeO_x/Cu(111) is only 0.31 eV. This value is also smaller than the corresponding values found for Cu nanoparticles supported on ZnO(000$\bar{1}$), 0.54 eV, or CeO_2(111), 0.39 eV.[22] Thus, CeO_x/Cu seems to be the best catalyst in terms of activity or apparent activation energy.

It must be pointed out that the ceria nanoparticles dispersed on Cu(111) do not have the same structure or

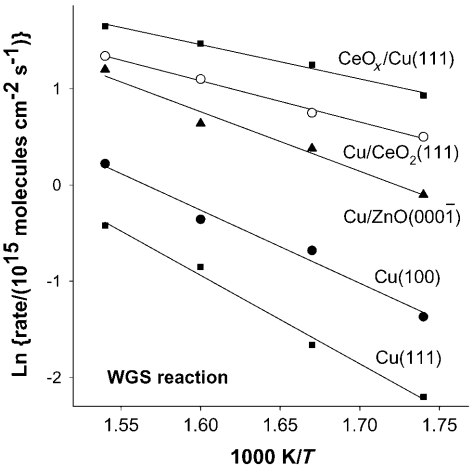

Figure 4. Arrhenius plot for the WGS reaction rate on clean Cu(111) and on a copper surface approximately 20 % covered by ceria. The CeO_x/Cu(111) surface was prepared by dosing Ce to Cu(111) at 650 K under an atmosphere of O_2 ($p \approx 5 \times 10^{-7}$ Torr). The data for Cu(100) and 0.5 monolayer (ML) of Cu deposited on CeO_2(111) and ZnO(000$\bar{1}$) surfaces were taken from Ref. [22].

electronic properties than the oxide support in Cu/CeO_2(111).[22] Figure 2 shows a typical Ce 3d XPS spectrum for a CeO_x/Cu(111) surface after performing the WGS reaction. The dominant oxidation state for cerium in a CeO_x/Cu(111) catalyst is "+3". This is not the case for a Cu/CeO_2(111) catalyst, where there are only a few O vacancies in the oxide support.[22] Cu L_3VV auger spectra taken after the WGS reaction, see bottom of Figure 2 for an example, indicated that metallic Cu formed part of the active phase of CeO_x/Cu(111). An identical result was found for Cu/CeO_2 catalysts.[8,22] When considering the catalytic activity of metallic copper, DF calculations show a substantial gain in WGS activity when going from extended surfaces to small or medium size nanoparticles.[10] The corner and edge atoms present in the copper nanoparticles facilitate the dissociation of water and the formation of key reaction intermediates in the WGS.[3,10] In spite of this feature, CeO_x/Cu(111) is more active than Cu/CeO_2(111), probably because of the special chemical properties of the ceria nanoparticles.

DF calculations were used to study the WGS reaction on CeO_x/Cu(111). The catalyst surface was represented by the model shown in Figure 5. Strictly speaking, this is a model for the small oxide particles seen in the STM images (CeO_x-I in Figure 1 and Figure 3). The model contains six atoms of Ce and 13 atoms of O. Since most of the oxygen atoms are shared between Ce and Cu, the average oxidation state of the Ce

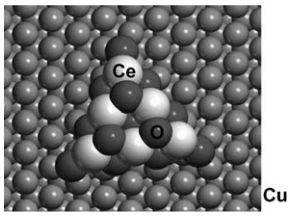

Figure 5. Model for a small Ce_6O_{13} particle on Cu(111).

atoms was close to "+3" as seen in plots for the density of occupied states. Thus, from an electronic viewpoint, the cerium cations in our model can be used to study the reactivity of the Ce^{3+} sites in small ceria particles (CeO_x-I) or in the interface between large ceria nanoparticles (CeO_x-II) and the copper substrate.

The partial dissociation of water ($H_2O_{ads} \rightarrow OH_{ads} + H_{ads}$) on Cu(111) was studied using the DF approach with different GGA functionals.[11,12] The reaction is endothermic ($\Delta E =$ 0.2–0.6 eV) with a large activation energy ($E_a = 0.9$–1.4 eV).[11,12] It is the rate determining step for the WGS on Cu(111).[10–14] Our DF calculations for the dissociation of H_2O on the Ce_6O_{13}/Cu(111) system of Figure 5 gave an exothermic ΔE value of -0.33 eV and point to an activation energy smaller than 0.35 eV. Thus, the oxide nanoparticles favor the energetics for the dissociation of water. This prediction has been verified by photoemission experiments in which we observed the partial dissociation of H_2O on CeO_x/Cu(111) surfaces at 300 K.

For the Cu(111) and CeO_x/Cu(111) systems in Figure 4, analysis of the surface after the WGS reaction showed weak or negligible XPS signals for formate and carbonate species. In a recent DF study for the WGS on Cu(111), a HOCO intermediate was seen as a transient species.[11] Figure 6

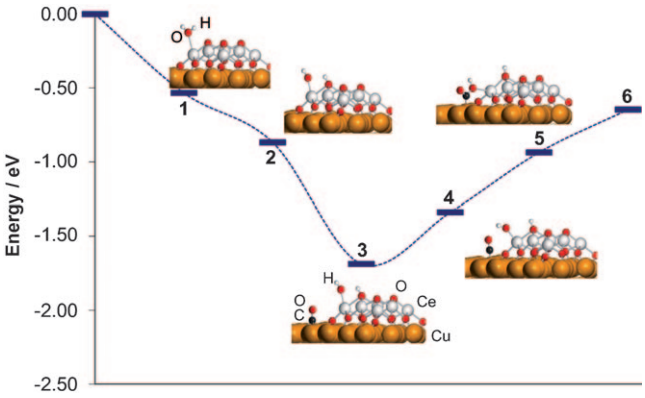

Figure 6. Reaction profile for the WGS on Ce_6O_{13}/Cu(111). Step 1: adsorption of water; Step 2: dissociation of water; Step 3: adsorption of CO; Step 4: approach of CO and OH; Step 5: formation of HOCO intermediate; Step 6: evolution of CO_2 and H_2.

displays a calculated reaction profile for the WGS on the Ce_6O_{13}/Cu(111) model system. The chemisorption of CO and the dissociation of water realease energy which can be used for the formation of HOCO and the final release of CO_2 and H_2. Although the dissociation of water occurs on the oxide nanoparticle the other steps of the reaction take place at the metal/oxide interface.

The CeO_x/Cu(111) system illustrates the important role that an oxide can play in the water-gas shift reaction. When optimizing the performance of copper-based WGS catalysts, the major emphasis is usually in controlling the oxidation state and morphology of the copper within the catalytic system.[1,2,4,8,22] The oxide is frequently seen as a simple

support for copper or as a secondary player in the catalysis. This is certainly valid in the case of Cu/ZnO[5–7,22] a common catalyst for industrial applications.[1] However, as a "support" for catalysts, ceria is more active than zinc oxide.[4,9,20,22,23] A comparison of the WGS activities of CeO_x/Cu(111) and Cu/CeO_2(111) shows that an optimization of the physical and chemical properties of the oxide component is as important as the optimization of the properties for the metal component. The key to the high catalytic activity of CeO_x/Cu(111) is in the nano size of the ceria particles and the effects of the metal/oxide interface. Powder catalysts with such an oxide/metal configuration can be synthesized using microemulsion techniques[15,24] and in principle can be used in practical applications.

Experimental Section

The microscopy studies were carried out in an Omicron variable temperature STM system.[18] W tips were used for imaging. Additional characterization studies were carried out in a system which combines a batch reactor and a UHV chamber.[18,22] The UHV chamber (base pressure $\approx 1\times10^{-10}$ Torr) was equipped with instrumentation for X-ray photoelectron spectroscopy (XPS), low-energy electron diffraction, ion-scattering spectroscopy (ISS), and thermal-desorption mass spectroscopy. XPS and Auger spectra were acquired using $Mg_{K\alpha}$ radiation. The Cu(111) surface was cleaned by several cycles of Ne^+ sputtering (1 keV, 30 min) and annealing (900 K, 5 min). Ce was deposited on Cu(111) using a metal evaporator.[18] The area of the copper surface covered by ceria was estimated using STM images or a combination of ISS and XPS. Before the ISS measurements, the CeO_x/Cu(111) surfaces were exposed to CO or CO/H_2O mixtures to remove the Cu_2O and expose the fraction of the copper surface not covered by ceria. The CeO_x/Cu(111) sample could be transferred between the UHV chamber and reactor without exposure to air. Typically, it was transferred to the batch reactor at ca. 298 K, the reactant gases were introduced (20 Torr of CO and 10 Torr of H_2O), and then the sample was rapidly heated to the reaction temperature (575, 600, 625, or 650 K). Product yields were analyzed by a gas chromatograph.[5,18,22] The amount of molecules produced was normalized by the active area exposed by the sample. In our reactor, a steady-state regime for the production of H_2 and CO_2 was reached after 2–3 min of reaction time.

Periodic DFT+U calculations were performed with the VASP code[25] using a $4\sqrt{3}\times4\sqrt{3}$ four-layer thick supercell to model the Cu(111) surface. The adlayer and first two layers of the copper slab were allowed to relax during the DFT geometry optimizations. We used the Perdew-Wang 91 GGA functional for exchange-correlation, the projector-augmented wave approach, and plane-waves with a cutoff energy set at 400 eV. We treated the Cu(3d,4s), Ce(4f,5s, 5p,5d,6s), C(2s,2p), O(2s,2p), and H(1s) electrons as valence states, while the remaining electrons were kept frozen as core states. Following previous studies,[26,27] we utilized a U_{eff} parameter with a value of 4.5 eV for Ce. This value is close to those used in studies for bulk ceria.[27] The introduction of the U_{eff} parameter in the DFT calculations was found to be essential to correctly reproduce the position for the occupied Ce 4f levels of ceria nanoparticles in the valence region.[26] (Additional details in Supporting Information.)

Received: July 17, 2009
Published online: September 24, 2009

Keywords: ceria · copper · heterogeneous catalysis · nanocatalysts · water-gas shift reaction

[1] a) R. Burch, *Phys. Chem. Chem. Phys.* **2006**, *8*, 5483; b) D. S. Newsome, *Catal. Rev. Sci. Eng.* **1980**, *21*, 275.
[2] R. Tavares-Figueiredo, A. L. Dantas-Ramos, H. Martins-Carvalho, J. L. G. Fierro, *Catal. Today* **2005**, *107*, 671.
[3] a) J. A. Rodriguez, P. Liu, X. Wang, W. Wen, J. Hanson, J. Hrbek, M. Pérez, J. Evans, *Catal. Today* **2009**, *143*, 45; b) J. A. Rodriguez, J. Evans, J. Graciani, J.-B. Park, P. Liu, J. Hrbek, J. Fdez. Sanz, *J. Phys. Chem. C* **2009**, *113*, 7364.
[4] Y. Li, Q. Fu, M. Flytzani-Stephanopoulos, *Appl. Catal. B* **2000**, *27*, 179.
[5] J. Nakamura, J. M. Campbell, C. T. Campbell, *J. Chem. Soc. Faraday Trans.* **1990**, *86*, 2725.
[6] C. V. Ovesen, P. Stoltze, J. K. Nørskov, C. T. Campbell, *J. Catal.* **1992**, *134*, 445.
[7] B. S. Clausen, G. Steffensen, B. Fabius, J. Villadsen, R. Feidenhansl, H. Topsøe, *J. Catal.* **1991**, *132*, 524.
[8] X. Wang, J. A. Rodriguez, J. C. Hanson, D. Gamarra, A. Martínez-Arias, M. Fernández-García, *J. Phys. Chem. B* **2006**, *110*, 428.
[9] a) S. Hilaire, X. Wang, T. Luo, R. J. Gorte, J. Wagner, *Appl. Catal. A* **2001**, *215*, 271; b) D. Tibiletti, E. A. B. de Graaf, S. P. Teh, G. Rothenberg, D. Farrusseng, C. Mirodatos, *J. Catal.* **2004**, *225*, 489.
[10] P. Liu, J. A. Rodriguez, *J. Chem. Phys.* **2007**, *126*, 164705.
[11] A. A. Gokhale, J. A. Dumesic, M. Mavrikakis, *J. Am. Chem. Soc.* **2008**, *130*, 1402.
[12] J. L. C. Fajín, F. Illas, J. R. B. Gomes, *J. Chem. Phys.* **2009**, *130*, 224702.
[13] C. T. Campbell, B. Koel, K. A. Daube, *J. Vac. Sci. Technol. A* **1987**, *5*, 810.
[14] C. A. Callaghan, S. A. Vilekar, I. Fishtik, R. Datta, *Appl. Catal. A* **2008**, *345*, 213.
[15] C. M. Y. Yeung, S. C. Tsang, *J. Phys. Chem. C* **2009**, *113*, 6074.
[16] F. Jensen, F. Besenbacher, I. Stensgaard, *Surf. Sci.* **1992**, *269/270*, 400.
[17] S. Ma, J. A. Rodriguez, J. Hrbek, *Surf. Sci.* **2008**, *602*, 3272.
[18] J. A. Rodriguez, S. Ma, P. Liu, J. Hrbek, J. Evans, M. Pérez, *Science* **2007**, *318*, 1757.
[19] A. Pfau, K. D. Schierbaum, *Surf. Sci.* **1994**, *321*, 71.
[20] a) A. Trovarelli, *Catal. Rev. Sci. Eng.* **1996**, *38*, 439; b) C. Loschen, A. Migan, S. T. Bromley, F. Illas, K. Neyman, *Phys. Chem. Chem. Phys.* **2008**, *10*, 5730.
[21] J. P. Espinós, J. Morales, A. Barranco, A. Caballero, J. P. Holgado, A. R. González-Elipe, *J. Phys. Chem. B* **2002**, *106*, 6921.
[22] J. A. Rodriguez, P. Liu, J. Hrbek, J. Evans, M. Pérez, *Angew. Chem.* **2007**, *119*, 1351; *Angew. Chem. Int. Ed.* **2007**, *46*, 1329.
[23] R. Si, M. Flytzani-Stephanopoulos, *Angew. Chem.* **2008**, *120*, 2926; *Angew. Chem. Int. Ed.* **2008**, *47*, 2884.
[24] L. D'Souza, R. Richards in *Synthesis Properties and Applications of Oxide Nanomaterials* (Eds.: J. A. Rodriguez, M. Fernández-García), Wiley, New York, **2007**, chap. 3.
[25] G. Kresse, J. Furthmuller, *Comput. Mater. Sci.* **1996**, *6*, 15.
[26] J. B. Park, J. Graciani, J. Evans, D. Stacchiola, S. Ma, P. Liu, A. Nambu, J. Fernández Sanz, J. Hrbek, J. A. Rodriguez, *Proc. Natl. Acad. Sci. USA* **2009**, *106*, 4975.
[27] a) S. Fabris, S. de Gironcoli, S. Baroni, G. Vicario, G. Balducci, *Phys. Rev. B* **2005**, *71*, 041102; b) C. Zhang, A. Michaelides, D. A. King, S. J. Jenkins, *J. Chem. Phys.* **2008**, *129*, 194708; c) C. Loschen, J. Carrasco, K. M. Neyman, F. Illas, *Phys. Rev. B* **2007**, *75*, 035115.

